The crystal structure of the TonB-dependent transporter YncD reveals a positively charged substrate binding site.

Rhys Grinter[a,b]# and Trevor Lithgow[b]

#To whom correspondence should be addressed: rhys.grinter@monash.edu

[a]School of Biological Sciences, Monash University, Clayton 3800, Victoria, Australia

[b]Infection and Immunity Program, Biomedicine Discovery Institute and Department of Microbiology, Monash University, Clayton 3800, Victoria, Australia

Keywords: YncD, Crystallography, Membrane Transport, Gram-Negative Bacteria, TonB-Dependent Transporter

Abstract

The outer membrane of Gram-negative bacteria is highly impermeable to hydrophilic molecules larger than 600 Da, protecting these bacteria from toxins present in the environment. In order to transport nutrients across this impermeable membrane, Gram-negative bacteria utilise a diverse family of outer-membrane proteins called TonB-dependent transporters. The majority of this family transport iron-containing substrates. However, it is becoming increasingly clear that TonB-dependent transporters target chemically diverse substrates. In this work, we investigate the structure and phylogenetic distribution of the TonB-dependent transporter YncD. We show that while YncD is present in some enteropathogens including *E. coli* and *Salmonella* spp., it is also widespread in Gamma and Betaproteobacteria of environmental origin. We determine the structure of YncD, showing that despite a distant evolutionary relationship, it shares structural features with the ferric-citrate transporter FecA, including a compact positively-charged substrate-binding site. Despite these shared features, we show that YncD does not contribute to the growth of *E. coli* in pure culture under-iron limiting conditions or with ferric-citrate as an iron source. Previous studies on transcriptional regulation in *E. coli* show that YncD is not induced under iron-limiting conditions and is unresponsive to the Ferric uptake regulator (Fur). These observations combined with the data we present, suggest that YncD is not responsible for the transport of an iron-containing substrate.

Introduction

The outer membrane of Gram-negative bacteria represents a formidable permeability barrier to hydrophilic molecules larger than ~600 Da (1). Hydrophilic molecules smaller than this diffusion limit cross the outer membrane through proteins called porins, which can be either promiscuous or substrate-specific (2). To import molecules that are too large for diffusion through outer-membrane porins, bacteria employ a diverse family of membrane proteins termed TonB-dependent transporters (TBDTs) (3). These transporters in the outer membrane are so named because they engage in active transport, the energy for which is provided by the TonB-ExbBD complex in the inner membrane, which spans the periplasm to interact with TBDTs (4,5). TBDTs are specific for a particular substrate, which they bind with high affinity in an extracellular binding pocket (6,7). This high-affinity binding allows TBDTs to capture molecules that are of low abundance in the environment, enabling bacteria to scavenge scarce nutrients (6). One such scarce nutrient is iron, which is the substrate for the majority of characterised TBDTs (3). Most iron-transporting TBDTs bind Fe^{3+} ions in complex with siderophores, organic molecules that bind metal ions with high affinity and are secreted by the bacteria or by competitors from the microbial community (8). In addition to importing Fe-siderophore complexes, some TBDTs harvest iron directly from proteins (9,10). These protein-binding TBDTs often target host proteins and are employed by pathogens to obtain iron during infections (11,12).

While many of the most intensively studied TBDTs import iron-containing substrates, it is becoming increasingly clear that members of the TBDT protein family are responsible for the import of chemically diverse substrates (13). Non-iron TBDT substrates range in size from free metal ions, like Cu^{2+} and Zn^{2+}, to cobalamin, polysaccharides, polypeptides, and small globular proteins (9,14-22). As functionally characterised TBDTs represent a small segment of this protein family, the extent of the substrate diversity of this family remains to be discovered.

The model bacterium *Escherichia coli* K12 possesses 9 TBDTs which target different substrates for import (7). The TBDTs FepA, CirA and Fiu transport Fe^{3+} containing catecholate siderophores (7,23,24), FhuA and FhuE transport Fe^{3+} containing hydroxamate siderophores

64 of fungal origin (6,25), FecA transports iron citrate (26), while BtuB targets cobalamin (16).
65 Recent research suggests that the TBDT YddB from *E. coli* K12 functions in the import of a
66 small iron-containing protein, although the exact nature of this substrate remains to be
67 identified (27). The final TBDT possessed by *E. coli* K12 is YncD, and the substrate for this
68 transporter remains unknown. The homolog of YncD in *Salmonella enterica* ssp. *enterica*
69 serovar Typhi has been shown to be important for virulence in a mouse model of infection
70 (28). As such, characterisation of YncD is important for understanding infections caused by
71 *Salmonella* and other enterobacterial pathogens that possess it.
72
73 In this study, we investigated the structure and phylogenetic distribution of YncD. Using a
74 comparative genomics approach, we show that YncD is present in members of
75 Enterobacteriaceae that form commensal or pathogenic associations with the human
76 intestine, and is more broadly present in environmental Proteobacterial isolates, including
77 species which are opportunistic pathogens of humans. We determined the crystal structure
78 of YncD demonstrating that it possesses a compact positively-charged extracellular substrate-
79 binding site that is characteristic of TBDTs that import negatively charged small-molecule
80 substrates. Finally, using an *E. coli* strain deficient in all iron transporting TBDTs we show that
81 YncD does not play a role in iron acquisition under laboratory conditions, providing further
82 evidence that this transporter does not transport an iron-containing substrate.
83
84
85

86 ## Results

87 ### The TonB-dependent transporter YncD is widespread in environmental bacteria

88 To determine the evolutionary relationship between YncD and other functionally
89 characterised TBDTs, we performed clustering analysis of these sequences based on pairwise
90 sequence similarity scores, using the program CLANS (29). This analysis reveals that YncD is
91 distantly related to other TBDTS of known function and does not form a cluster with any of
92 these sequences (Figure 1A). This analysis shows that while YncD is most closely related to
93 the TBDTs FecA and BtuB, this reflects only 21% and 18% sequence identity, respectively.
94
95 To gain insight into the distribution of YncD in Gram-negative bacteria, we interrogated the
96 Uniprot reference proteomes for YncD homologues with the HMMER search algorithm
97 (30,31). An initial sequence similarly E-value cut-off of $1x10^{-50}$ was used to capture all YncD
98 sequences present in the database. To remove false-positive non-YncD sequences from this
99 dataset, we subsequently clustered the sequences using CLANS (29) with an E-value cut-off of
100 $1x10^{-130}$. The largest sequence cluster had 359 distinct sequences including YncD from *E. coli*
101 and was extracted for curation and analysis (Table S1, Figure S1A). Partial sequences were
102 removed from this dataset, yielding 331 sequences. These were reclustered with an E-value
103 cut-off of 0, revealing several distinct sub-sets within the YncD protein sub-family (Figure
104 S1B). A multiple sequence alignment of these diverse YncD sequences was then performed
105 revealing that they share amino acid sequence identities ranging between 33 and 99 % (Table
106 S2, Data S1), and highlighted a number of conserved regions. Most notably the region of the
107 corresponding in amino acids 79-150 of YncD from *E. coli* is highly conserved (Data S1). This
108 region encompasses the extracellular loops of the N-terminal plug domain of the transporter,
109 known to mediate substrate binding, suggesting that the YncD homologues identified target a
110 chemically analogous substrate.
111
112 To explore potential niche-specific functions associated with YncD, we interrogated genome
113 metadata from those bacteria identified in the YncD HMMER search. The environment of
114 isolation of 105 YncD-containing species was determined, with all bacteria belonging to
115 either the gamma- or beta-proteobacteria (Table S1). While some of these bacterial species
116 were isolated from a human host (largely Enterobacteriaceae associated with the gut or

117 Pseudomonadales associated with respiratory infection), the majority of YncD-containing
118 bacteria were environmental isolates (Figure 1B). The environmental isolates originated from
119 soil, sediment or water samples (Figure 1C). The widespread distribution of YncD in
120 environmental isolates, and its absence from most specialist bacterial pathogens, would be
121 most consistent with YncD playing a role in the acquisition of a molecule produced by the
122 microbial community.
123

124 **The crystal structure of YncD from *E. coli* reveals a positively charged substrate-binding site**

125 To gain insight into the evolutionary relationship between YncD and other TBDTs and to
126 provide insight into the nature of the YncD substrate, we solved the crystal structure of YncD
127 by X-ray crystallography. Crystals of YncD from *E. coli* were prepared and diffraction was
128 collected to 3.2 Å (Table 1). Molecular replacement using the closest YncD homologue FecA
129 (PDB ID: 1KMO, 1KMP) proved unsuccessful (26). To obtain experimental phases, YncD
130 crystals were soaked with potassium tetranitroplatinate and anomalous diffraction was
131 collected to 3.5 Å (Table 1). Phases were obtained for this dataset using single-wavelength
132 anomalous dispersion (SAD) phasing, with an anomalous substructure of 2 high occupancy
133 and 1 low occupancy platinum atoms located (Figure S3). An initial model of YncD was build
134 using maps from this dataset and utilised to obtain phases for the higher resolution dataset
135 by molecular replacement. The structure of YncD was then built and refined using the native
136 3.2 Å data (Table 1).
137

138 As expected, based on other members of the TBDT family, structurally YncD consists of at 22
139 stranded transmembrane β-barrel, which is occluded by a globular N-terminal plug domain
140 (Figure 2A, B). The Dali server was utilised to search the protein databank (PDB) for structural
141 homologues to YncD (32), revealing that consistent with our sequence analysis the closest
142 structural homologue to YncD is FecA (Table S3). Despite the low sequence identity of 21 %
143 between YncD and FecA, these proteins share a backbone atom root mean square deviation
144 (RMSD) of 2.2 Å. Consistent with this, the extracellular loop length, secondary and tertiary
145 structure is relatively well conserved between the two proteins, compared to the more
146 distantly related TBDT FhuE (Figure 2C, Figure S2).
147

148 Previous analysis of the structure of diverse TBDTs in complex with their substrates revealed
149 the location of a conserved substrate-binding site in these transporters (7). Based on this
150 analysis we identified a compact substrate-binding site formed by the extracellular loops of
151 YncD in our structure (Figure 3A). Analysis of sequence conservation among YncD
152 homologues using the program Consurf (33) and our alignment of YncD sequences revealed
153 that the residues that constitute this binding pocket are well conserved in the YncD
154 homologues, suggesting they play an important role in transporter function (Figure 1B, C,
155 Data S1). These conserved residues include a number of arginine, glutamine and lysine
156 residues that give the substrate-binding site of YncD a highly positive charged, based on a
157 calculated electrostatic surface (Figure 3B-D). Electrostatic analysis of the structure of FecA
158 shows that this distant YncD homologue also possesses a highly positively charged substrate-
159 binding site (Figure 3C). In FecA, several arginine and glutamine residues, which give the
160 substrate-binding site its positive character, are responsible for coordinating the carboxylic
161 acid groups of the Fe-citrate complex, and thus are important for substrate binding by FecA
162 (Figure 3C) (26). Superimposition of the FecA-Fe-Citrate complex with YncD places Fe-citrate
163 ligand centrally in the positively charged substrate binding site of YncD (Figure 3C). The
164 similarities between the character of the substrate bindings sites of YncD and FecA suggest
165 that despite their differences they may target chemically similar substrates.
166

167 **YncD does not import ferric citrate or support growth of *E. coli* during iron limitation in pure**
168 **culture**

169 To test the hypothesis that YncD could support growth under iron-limiting conditions and
170 specifically that it imports ferric citrate, we monitored the growth of an isogenic *E. coli* strain
171 with and without YncD. Because TBDT iron-uptake systems are highly redundant, the *yncD*
172 gene was deleted in a strain which is deficient in the 7 TBDTs involved in iron-uptake (Figure
173 S4) (7). This ΔTBDT strain grows poorly under iron-limiting conditions (6), making any
174 additional iron-acquisition defect easier to discern. In M9 minimal media, the growth of the
175 ΔTBDT +/- *yncD* was identical, demonstrating that YncD does not play a role in iron
176 acquisition under these conditions (Figure 4A). Since there is some residual free iron in M9
177 minimal media, the available iron was chelated with the addition of citrate or the monomeric
178 catecholate compound 2,3-dihydroxybenzoic acid (DHB). As the ΔTBDT strain lacks the outer
179 membrane transporters required to import these substrates, they limit the exogenous iron

180 available to the bacteria. Accordingly, the growth of *E. coli* ΔTBDT was somewhat reduced in
181 the presence of DHB and drastically reduced in the presence of citrate (Figure 4B). Deletion
182 of *yncD* in this strain had no further effect on growth, demonstrating that YncD does not play
183 a role in importing Fe-citrate or Fe-DHB under these conditions (Figure 4B). As expected
184 growth of wildtype *E. coli* BW25113, which possesses TBDTs for both ferric-citrate (FecA) and
185 Fe-DHB (Fiu, CirA, FepA) import (7,26) was identical in the presence or absence of these
186 compounds (Figure 4C).

187

188 ## Discussion

189 Determination of the function of proteins is one of the most challenging aspects of modern
190 protein biochemistry. The expansion of genomic and metagenomic sequencing data has
191 provided a wealth of proteins sequences, most of which are only partially characterised or of
192 completely unknown function. Despite its difficulty, determining the function of novel
193 proteins is invaluable, as without a robust understanding of the functional capacity of an
194 organism's proteome it is difficult to accurately predict its metabolic capabilities, physiology
195 or lifestyle.

196

197 In this work, we show that YncD is a TBDT which is only distantly related to previously
198 characterised members of this family and that YncD is widespread in gamma- and beta-
199 proteobacteria. The crystal structure of YncD shows common structural features with the
200 ferric-citrate transporter FecA, but from growth assays, YncD appears not to transport ferric-
201 citrate. The structure of YncD represents the final structure of the 9 TBDTs possessed by the
202 model bacterium *E. coli* K12 (6,7,23,26,34-36). This structure improves our understanding of
203 the structural variation and similarities that exist in the TBDT family and paves the way for
204 future studies addressing the function of YncD.

205

206 Seven of the nine TBDTs present in *E. coli* are involved in iron acquisition. All of these
207 transporters are regulated by the Ferric uptake regulator (Fur) and are induced under iron-
208 limiting conditions (37). BtuB, which imports the non-iron containing substrate cobalamin, is
209 neither Fur regulated or induced under iron limiting conditions (37,38). Interestingly, like

210 BtuB, YncD is neither Fur regulated or upregulated under iron-limiting conditions, suggesting
211 that it may not function in the import of an iron-containing substrate (37,38). While the
212 specific substrate transported by YncD remains to be determined, this work provides a
213 number of clues and avenues for further research towards its identification. Based on its
214 compact negatively-charged extracellular binding site, the substrate of YncD is likely to be
215 relatively small and negatively charged.
216

217 As YncD is prevalent in bacterial species from soil and aquatic communities, its substrate is
218 likely produced by members of these ecological communities. In addition, the impact of YncD
219 on virulence phenotypes in *Salmonella* Typhi suggest that it is also a molecule which is
220 relevant in a human host-context (28). Based on these considerations and structural
221 parameters in the ligand-binding site, possible substrates for YncD would include molecules
222 containing negatively charged phosphate groups. Other members of the TBDT family have
223 been previously been implicated in thiamine pyrophosphate import through comparative
224 genomics (39). Alternatively, YncD may import an organic acid containing compound in
225 complex with a non-ferrous metal ion (26).

226

227 The importance of YncD for virulence in *Salmonella* Typhi (28), makes understanding the
228 function of this transporter an important question for medical microbiology. Understanding
229 the substrate of YncD and the role of this compound in bacterial virulence will improve our
230 fundamental understanding of infection by this bacterium and provide a potential target for
231 therapeutic intervention.

232

233 Methods

234 YncD Homologue Identification and Analysis

235 To determine the evolutionary relationship between YncD and other TBDTs of known structure
236 and/or function these sequences were classified by an all-against-all BLAST clustering algorithm,
237 based on pairwise similarities. The resulting data set was visualized with CLANS with an E-value cut
238 off of 1×10^{-10} (29).

239 To identify YncD sequences in available bacterial genomes, a HMMER search was performed on the
240 Uniprot reference proteomes database using YncD as the search sequence (30,31). An E-value cut-off
241 of $1x10^{-50}$ applied to hits. This search yielded a total of 568 YncD homologue sequences. These
242 sequences were classified by an all-against-all BLAST clustering algorithm, based on pairwise
243 similarities. The resulting data set was visualized with CLANS with an E value cut off of 1×10^{-130}.
244 Sequence clusters were identified in CLANS using a network-based algorithm, with a minimum group
245 size of 10 (29). The largest sequence cluster from this clustering contained 359 sequences, including
246 YncD from *E. coli* and designated the YncD group. This group was isolated and subjected to further
247 clustering with an E value cut off of 0. A multiple sequence alignment was performed on 331 full-
248 length sequences from the YncD group using the clustal algorithm (40). Environment or host of
249 isolation for a subset of YncD sequences (105 sequences) was determined from genome metadata
250 from the Ensemble and Uniprot databases (41,42).

251

252 YncD Expression and Purification

253 The open reading frame encoding YncD was amplified by PCR from *E. coli* BW25113 using primers
254 containing 5' BamHI and 3' XhoI restriction sites (Forward: CCATCGGATCCGGCTGA
255 TGAACAGACTATGATTGTC, Reverse: CCATCCTCGAGTTACTCAAATCTCCACGCAATATTCAT). This YncD
256 open reading frame was then cloned into a modified pET20b vector with a PelB signal sequence,
257 followed by an N-terminal 10 × His-tag and TEV cleavage site, via restriction digestion and ligation.
258 The resulting vector was transformed into *E. coli* BL21 (DE3) C41 cells (43). Protein expression was
259 performed in terrific broth (12 g tryptone, 24 g yeast extract, 61.3 g K_2HPO_4, 11.55 g KH_2PO_4, 10 g
260 glycerol) with 100 $mg.ml^{-1}$ ampicillin for selection. Cells were grown at 37 °C until OD_{600} of 1.0,
261 induced with 0.3 mM IPTG, and grown for a further 14 hours at 25 °C. Cells were harvested by
262 centrifugation and lysed using a cell disruptor (Emulseflex) in Lysis Buffer (50 mM Tris, 200 mM NaCl
263 [pH 7.9]) in the presence of 0.1 $mg.ml^{-1}$ Lysozyme, 0.05 $mg.ml^{-1}$ DNAse1 and complete protease
264 cocktail inhibitor tablets (Roche).

265 The resulting lysate was clarified by centrifugation at 10,000 g for 10 min, the supernatant from this
266 low-speed spin was then centrifuged to 1 h at 100,000 g to isolate a membrane fraction. The
267 supernatant was decanted, and the membrane pellet was suspended in lysis buffer using a tight-
268 fitting homogeniser. The resuspended membranes were solubilised by the addition of 10 % Elugent
269 (Santa Cruz Biotechnology) and incubated with gentle stirring at room temperature for 20 min. The
270 solubilised membrane protein fraction was clarified by centrifugation at 20,000 g for 10 min. The
271 supernatant containing the solubilized proteins was applied to Ni-agarose resin equilibrated in Ni-

272 binding buffer DDM (50 mM Tris, 500 mM NaCl, 20 mM Imidazole, 0.03% Dodecylmaltoside (DDM)
273 [pH7.9]). The resin was washed with 10-20 column volumes of Ni binding buffer DDM before elution
274 of the protein with a step gradient of, 10, 25 and 50, 100 % Ni gradient buffer DDM (50 mM Tris, 500
275 mM NaCl, 1 M Imidazole, 0.03 % DDM [pH7.9]). YncD eluted at the 50 and 100 % gradient steps.
276 Eluted fractions containing YncD were pooled and applied to a 26/600 S200 Superdex size exclusion
277 column equilibrated in SEC buffer DDM (50 mM Tris, 200 mM NaCl, 0.03 % DDM [pH 7.9]). To
278 exchange YncD into the detergent Octyl β-D-glucopyranoside (βOG) for crystallographic and
279 biochemical analysis, SEC fractions containing YncD were pooled and applied to Ni-agarose resin,
280 equilibrated in βOG buffer (50 mM Tris, 200 mM NaCl, 0.8 % βOG [pH 7.9]). The resin was washed
281 with 10 column volumes of βOG buffer before elution with βOG buffer + 250 mM imidazole. Fractions
282 containing YncD were pooled, and 6 × His-tagged TEV protease (final concentration 2 $mg.ml^{-1}$) and DTT
283 (final concentration 1 mM) were added. This solution was then dialysed against of βOG buffer at 4-6h
284 at 20 °C to allow TEV cleavage of the 10 × his-tag from YncD and removal of excess imidazole. The
285 sample was then applied to Ni-agarose resin to remove TEV protease and the cleaved histidine-
286 containing peptide. The flow-through containing YncD from this step was collected, concentrated to
287 10 $mg.ml^{-1}$ in a 30 kDa cut-off centrifugal concentrator, snap-frozen and stored at -80 °C.

288

289 YncD Crystallisation, Data Collection and Structure Solution

290 Purified YncD in βOG was screened for crystallisation conditions using commercially available screens
291 (approximately 600 conditions). Crystals grew in a number of conditions, with a condition containing
292 0.2 M Ca acetate, 0.10 M Tris pH 8.5 and 20 % PEG 3000 chosen for optimisation. Concentration and
293 pH grid screening was performed yielding an optimised crystallisation conditions containing 0.17 M Ca
294 acetate, 0.10 M Tris pH 7.0 and 16 % PEG 3000. Crystals from this condition were looped,
295 crystallisation solution was removed by wicking and crystals were flash-cooled in liquid N_2. Diffraction
296 data were collected at 100 K at the Australian synchrotron and processed in the space group $P2_122_1$
297 to 3.2 Å. Molecular replacement of this dataset using the structures of various TBDTs as a starting
298 model failed and so soaking was performed to obtain a heavy atom derivative. Using a fine
299 acupuncture needle a small quantity of potassium tetranitroplatinate salt was added to the drop
300 containing YncD crystals, the well was resealed and crystal incubated for 60 minutes. These crystals
301 were then were looped, crystallisation solution was removed by wicking and crystals were flash-
302 frozen in liquid N_2. Data was collected from the potassium tetranitroplatinate soaked crystals at 100 K
303 at the Australian synchrotron using a wavelength of 0.987 Å, with crystals diffracting to 3.5 Å. A heavy
304 atom search was performed by SAD using Shelx within the CCP4 software package (44,45). Three

305 heavy atom sites were identified, which were provided to Autosol withing the Phenix software
306 package for phasing and density modification (46). An initial structure of YncD was constructed using
307 these experimentally-phased density modified maps using Coot (47). This model was used for
308 molecular replacement of the 3.2 Å native data using phaser (48). The model of YncD was then build
309 and refined using Coot, Phenix package and Buster (46,47,49).

310

311 ***E. coli ΔyncD*** Mutant Generation and Growth Analysis

312 The *E. coli* BW25113 *ΔyncD* mutant strain was created using the λ Red system (50). A Kanamycin-
313 resistance cassette flanked by 300 bp of genomic DNA either side of the chromosomal location of
314 *yncD* was amplified by PCR (primers: F: AAACAGGCTATTTCGCTTAGCGA, R:
315 GAACCTAACAGTAATGAACCACG using the specific mutant from the *E. coli* Keio collection (51) as a
316 template, generating the yncD-Kan KO cassette. *E. coli* ΔTBDT (6) was transformed with the λ Red
317 recombinase plasmid pKD46 (50) and grown at 30 °C (LB broth + 100 $\mu g.ml^{-1}$ ampicillin + 100 uM
318 $Fe(II)SO_4$) to an OD600 nm of 0.1 before λ Red recombinase was induced by the addition of 0.2% L-
319 arabinose. The culture was then grown at 30 °C until an OD600 nm of 0.6–0.8 was attained and were
320 transformed with the yncD-Kan KO cassette using the room-temperature electroporation method
321 (52). Briefly, bacterial cells were isolated by centrifugation at 3000 g for 3 min and washed twice with
322 a volume of sterile 10% glycerol equal to the volume of culture used. The cells were then
323 resuspended in 10% glycerol to a volume of 1/15 of that of the culture. The yncD-Kan KO cassette
324 DNA (100–500 ng) was then added to 100 µl of the resuspended bacteria and the mixture was
325 electroporated. 1 ml of LB broth was added to the cells post-electroporation, and the culture was
326 recovered at 37°C for 1 h before plating onto LB agar + 30 $\mu g\ ml^{-1}$ kanamycin + 100 uM $Fe(II)SO_4$. PCR
327 was used to validate that colonies did indeed have the KanR cassette in place of the gene of interest.

328 To remove the KanR gene and generate a "clean" *yncD* deletion, the mutant strain was transformed
329 with the plasmid pCP20 (53) containing the `flippase cassette'. Cells were grown at 30 °C under either
330 ampicillin (100 $\mu g\ ml^{-1}$) or chloramphenicol (30 $\mu g\ ml^{-1}$) selection to maintain the plasmid. A single
331 colony of the mutant pCP20-containing strain was used to inoculate 1 ml LB broth + 100 uM $Fe(II)SO_4$
332 (no selection). The culture was grown overnight at 43°C to activate expression of the flippase gene.
333 This culture was then subjected to tenfold serial dilution in sterile LB and plated onto LB agar + 100
334 uM $Fe(II)SO_4$ with no selection. The resulting colonies were patched onto LB agar containing
335 kanamycin, chloramphenicol or no selection. PCR was used to validate colonies that, while unable to
336 grow in the presence of kanamycin or chloramphenicol, grew in the absence of selection and had no
337 remnant of the KanR cassette in the deletion of *yncD*.

338 *E. coli* ΔTBDT, *E. coli* ΔTBDT/*ΔyncD* and wildtype *E. coli* BW25113 were grown in LB broth until
339 stationary phase. These cultures were used to inoculate 20 ml of M9 minimal media +/- 10 mM citrate
340 or +/- 100 µM 2,3-Dihydrobenzoic acid, to an OD600nm of 0.05. Cultures were grown at 37 °C with
341 shaking and the rate of growth was quantified by measuring OD600nm at hourly intervals.

342

343

344

345

346

References

1. van den Berg, B., Prathyusha Bhamidimarri, S., Dahyabhai Prajapati, J., Kleinekathöfer, U., and Winterhalter, M. (2015) Outer-membrane translocation of bulky small molecules by passive diffusion. *Proceedings of the National Academy of Sciences* **112**, E2991-E2999
2. Vergalli, J., Bodrenko, I. V., Masi, M., Moynié, L., Acosta-Gutiérrez, S., Naismith, J. H., Davin-Regli, A., Ceccarelli, M., van den Berg, B., and Winterhalter, M. (2019) Porins and small-molecule translocation across the outer membrane of Gram-negative bacteria. *Nat. Rev. Microbiol.*, 1-13
3. Noinaj, N., Guillier, M., Barnard, Travis J., and Buchanan, S. K. (2010) TonB-Dependent Transporters: Regulation, Structure, and Function. *Annual Review of Microbiology* **64**, 43-60
4. Maki-Yonekura, S., Matsuoka, R., Yamashita, Y., Shimizu, H., Tanaka, M., Iwabuki, F., and Yonekura, K. (2018) Hexameric and pentameric complexes of the ExbBD energizer in the Ton system. *Elife* **7**
5. Celia, H., Noinaj, N., Zakharov, S. D., Bordignon, E., Botos, I., Santamaria, M., Barnard, T. J., Cramer, W. A., Lloubes, R., and Buchanan, S. K. (2016) Structural insight into the role of the Ton complex in energy transduction. *Nature*
6. Grinter, R., and Lithgow, T. (2019) Determination of the molecular basis for coprogen import by Gram-negative bacteria. *IUCrJ* **6**
7. Grinter, R., and Lithgow, T. (2019) The structure of the bacterial iron–catecholate transporter Fiu suggests that it imports substrates via a two-step mechanism. *Journal of Biological Chemistry* **294**, 19523-19534
8. Chu, B., Garcia-Herrero, A., Johanson, T., Krewulak, K., Lau, C., Peacock, R., Slavinskaya, Z., and Vogel, H. (2010) Siderophore uptake in bacteria and the battle for iron with the host; a bird's eye view. *Biometals* **23**, 601-611
9. Grinter, R., Josts, I., Mosbahi, K., Roszak, A. W., Cogdell, R. J., Bonvin, A. M., Milner, J. J., Kelly, S. M., Byron, O., and Smith, B. O. (2016) Structure of the bacterial plant-ferredoxin receptor FusA. *Nature communications* **7**
10. Noinaj, N., Easley, N. C., Oke, M., Mizuno, N., Gumbart, J., Boura, E., Steere, A. N., Zak, O., Aisen, P., Tajkhorshid, E., Evans, R. W., Gorringe, A. R., Mason, A. B., Steven, A. C., and Buchanan, S. K. (2012) Structural basis for iron piracy by pathogenic Neisseria. *Nature* **483**, 53-58
11. Leduc, I., Banks, K. E., Fortney, K. R., Patterson, K. B., Billings, S. D., Katz, B. P., Spinola, S. M., and Elkins, C. (2008) Evaluation of the Repertoire of the TonB-Dependent Receptors of Haemophilus ducreyi for Their Role in Virulence in Humans. *Journal of Infectious Diseases* **197**, 1103-1109
12. Cornelissen, C. N., Kelley, M., Hobbs, M. M., Anderson, J. E., Cannon, J. G., Cohen, M. S., and Sparling, P. F. (1998) The transferrin receptor expressed by gonococcal strain FA1090 is required for the experimental infection of human male volunteers. *Molecular Microbiology* **27**, 611-616
13. Schauer, K., Rodionov, D. A., and de Reuse, H. (2008) New substrates for TonB-dependent transport: do we only see the 'tip of the iceberg'? *Trends in biochemical sciences* **33**, 330-338
14. Grinter, R., Milner, J., and Walker, D. (2012) Ferredoxin containing bacteriocins suggest a novel mechanism of iron uptake in *Pectobacterium* spp. *PLoS ONE* **7**, e33033
15. Grinter, R., Hay, I. D., Song, J., Wang, J., Teng, D., Dhanesakaran, V., Wilksch, J. J., Davies, M. R., Littler, D., and Beckham, S. A. (2018) FusC, a member of the M16 protease family acquired by bacteria for iron piracy against plants. *PLoS Biol.* **16**, e2006026
16. Chimento, D. P., Mohanty, A. K., Kadner, R. J., and Wiener, M. C. (2003) Substrate-induced transmembrane signaling in the cobalamin transporter BtuB. *Nature Structural & Molecular Biology* **10**, 394
17. Yoneyama, H., and Nakae, T. (1996) Protein C (OprC) of the outer membrane of Pseudomonas aeruginosa is a copper-regulated channel protein. *Microbiology* **142**, 2137-2144

398 18. Calmettes, C., Ing, C., Buckwalter, C. M., El Bakkouri, M., Lai, C. C.-L., Pogoutse, A., Gray-
399 Owen, S. D., Pomès, R., and Moraes, T. F. (2015) The molecular mechanism of Zinc acquisition
400 by the neisserial outer-membrane transporter ZnuD. *Nature communications* **6**, 7996
401 19. Bolam, D. N., and van den Berg, B. (2018) TonB-dependent transport by the gut microbiota:
402 novel aspects of an old problem. *Current opinion in structural biology* **51**, 35-43
403 20. Glenwright, A. J., Pothula, K. R., Bhamidimarri, S. P., Chorev, D. S., Baslé, A., Firbank, S. J.,
404 Zheng, H., Robinson, C. V., Winterhalter, M., Kleinekathöfer, U., Bolam, D. N., and van den
405 Berg, B. (2017) Structural basis for nutrient acquisition by dominant members of the human
406 gut microbiota. *Nature* **541**, 407-411
407 21. Madej, M., White, J. B., Nowakowska, Z., Rawson, S., Scavenius, C., Enghild, J. J., Bereta, G. P.,
408 Pothula, K., Kleinekathoefer, U., and Baslé, A. (2019) Dynamic oligopeptide acquisition by the
409 RagAB transporter from Porphyromonas gingivalis. *bioRxiv*, 755678
410 22. Grinter, R., Josts, I., Zeth, K., Roszak, A. W., McCaughey, L. C., Cogdell, R. J., Milner, J. J., Kelly,
411 S. M., Byron, O., and Walker, D. (2014) Structure of the atypical bacteriocin pectocin M2
412 implies a novel mechanism of protein uptake. *Molecular microbiology* **93**, 234-246
413 23. Buchanan, S. K., Smith, B. S., Venkatramani, L., Xia, D., Esser, L., Palnitkar, M., Chakraborty, R.,
414 Van Der Helm, D., and Deisenhofer, J. (1999) Crystal structure of the outer membrane active
415 transporter FepA from Escherichia coli. *Nature Structural & Molecular Biology* **6**, 56
416 24. Nikaido, H., and Rosenberg, E. Y. (1990) Cir and Fiu proteins in the outer membrane of
417 Escherichia coli catalyze transport of monomeric catechols: study with beta-lactam antibiotics
418 containing catechol and analogous groups. *Journal of bacteriology* **172**, 1361-1367
419 25. Pawelek, P. D., Croteau, N., Ng-Thow-Hing, C., Khursigara, C. M., Moiseeva, N., Allaire, M., and
420 Coulton, J. W. (2006) Structure of TonB in complex with FhuA, *E. coli* outer membrane
421 receptor. *Science* **312**, 1399-1402
422 26. Ferguson, A. D., Chakraborty, R., Smith, B. S., Esser, L., Van Der Helm, D., and Deisenhofer, J.
423 (2002) Structural basis of gating by the outer membrane transporter FecA. *Science* **295**, 1715-
424 1719
425 27. Grinter, R., Leung, P. M., Wijeyewickrema, L. C., Littler, D., Beckham, S., Pike, R. N., Walker, D.,
426 Greening, C., and Lithgow, T. (2019) Protease-associated import systems are widespread in
427 Gram-negative bacteria. *PLoS Genet.* **15**
428 28. Xiong, K., Chen, Z., Xiang, G., Wang, J., Rao, X., Hu, F., and Cong, Y. (2012) Deletion of yncD
429 gene in Salmonella enterica ssp. enterica serovar Typhi leads to attenuation in mouse model.
430 *FEMS microbiology letters* **328**, 70-77
431 29. Frickey, T., and Lupas, A. (2004) CLANS: a Java application for visualizing protein families
432 based on pairwise similarity. *Bioinformatics* **20**, 3702-3704
433 30. Chen, C., Natale, D. A., Finn, R. D., Huang, H., Zhang, J., Wu, C. H., and Mazumder, R. (2011)
434 Representative Proteomes: A Stable, Scalable and Unbiased Proteome Set for Sequence
435 Analysis and Functional Annotation. *PLoS ONE* **6**, e18910
436 31. Finn, R. D., Clements, J., and Eddy, S. R. (2011) HMMER web server: interactive sequence
437 similarity searching. *Nucleic Acids Res.* **39**, W29-W37
438 32. Holm, L., and Laakso, L. M. (2016) Dali server update. *Nucleic acids research* **44**, W351-W355
439 33. Ashkenazy, H., Abadi, S., Martz, E., Chay, O., Mayrose, I., Pupko, T., and Ben-Tal, N. (2016)
440 ConSurf 2016: an improved methodology to estimate and visualize evolutionary conservation
441 in macromolecules. *Nucleic acids research* **44**, W344-W350
442 34. Buchanan, S. K., Lukacik, P., Grizot, S., Ghirlando, R., Ali, M. M., Barnard, T. J., Jakes, K. S.,
443 Kienker, P. K., and Esser, L. (2007) Structure of colicin I receptor bound to the R-domain of
444 colicin Ia: implications for protein import. *The EMBO journal* **26**, 2594-2604
445 35. Locher, K. P., Rees, B., Koebnik, R., Mitschler, A., Moulinier, L., Rosenbusch, J. P., and Moras,
446 D. (1998) Transmembrane signaling across the ligand-gated FhuA receptor: crystal structures
447 of free and ferrichrome-bound states reveal allosteric changes. *Cell* **95**, 771-778

36. Grinter, R., Leung, P. M., Wijeyewickrema, L. C., Littler, D., Beckham, S., Pike, R. N., Walker, D., Greening, C., and Lithgow, T. (2019) Protease-associated import systems are widespread in Gram-negative bacteria. *PLoS Genetics* **15**, e1008435
37. Seo, S. W., Kim, D., Latif, H., O'Brien, E. J., Szubin, R., and Palsson, B. O. (2014) Deciphering Fur transcriptional regulatory network highlights its complex role beyond iron metabolism in Escherichia coli. *Nat. Commun.* **5**, 4910
38. McHugh, J. P., Rodríguez-Quiñones, F., Abdul-Tehrani, H., Svistunenko, D. A., Poole, R. K., Cooper, C. E., and Andrews, S. C. (2003) Global iron-dependent gene regulation in Escherichia coli A new mechanism for iron homeostasis. *J. Biol. Chem.* **278**, 29478-29486
39. Rodionov, D. A., Vitreschak, A. G., Mironov, A. A., and Gelfand, M. S. (2002) Comparative genomics of thiamin biosynthesis in procaryotes New genes and regulatory mechanisms. *Journal of Biological chemistry* **277**, 48949-48959
40. Larkin, M. A., Blackshields, G., Brown, N., Chenna, R., McGettigan, P. A., McWilliam, H., Valentin, F., Wallace, I. M., Wilm, A., and Lopez, R. (2007) Clustal W and Clustal X version 2.0. *bioinformatics* **23**, 2947-2948
41. Hubbard, T., Barker, D., Birney, E., Cameron, G., Chen, Y., Clark, L., Cox, T., Cuff, J., Curwen, V., and Down, T. (2002) The Ensembl genome database project. *Nucleic Acids Res.* **30**, 38-41
42. Apweiler, R., Bairoch, A., Wu, C. H., Barker, W. C., Boeckmann, B., Ferro, S., Gasteiger, E., Huang, H., Lopez, R., and Magrane, M. (2004) UniProt: the universal protein knowledgebase. *Nucleic Acids Res.* **32**, D115-D119
43. Miroux, B., and Walker, J. E. (1996) Over-production of proteins in Escherichia coli: mutant hosts that allow synthesis of some membrane proteins and globular proteins at high levels. *Journal of molecular biology* **260**, 289-298
44. Sheldrick, G. M. (2008) A short history of SHELX. *Acta Crystallographica Section A: Foundations of Crystallography* **64**, 112-122
45. Winn, M. D., Ballard, C. C., Cowtan, K. D., Dodson, E. J., Emsley, P., Evans, P. R., Keegan, R. M., Krissinel, E. B., Leslie, A. G., and McCoy, A. (2011) Overview of the CCP4 suite and current developments. *Acta Crystallographica Section D: Biological Crystallography* **67**, 235-242
46. Adams, P. D., Afonine, P. V., Bunkoczi, G., Chen, V. B., Davis, I. W., Echols, N., Headd, J. J., Hung, L.-W., Kapral, G. J., Grosse-Kunstleve, R. W., McCoy, A. J., Moriarty, N. W., Oeffner, R., Read, R. J., Richardson, D. C., Richardson, J. S., Terwilliger, T. C., and Zwart, P. H. (2010) PHENIX: a comprehensive Python-based system for macromolecular structure solution. *Acta Crystallogr. Sect. D.* **66**, 213-221
47. Emsley, P., Lohkamp, B., Scott, W. G., and Cowtan, K. (2010) Features and development of Coot. *Acta Crystallogr. Sect. D.* **66**, 486-501
48. McCoy, A. J., Grosse-Kunstleve, R. W., Adams, P. D., Winn, M. D., Storoni, L. C., and Read, R. J. (2007) Phaser crystallographic software. *Journal of applied crystallography* **40**, 658-674
49. Smart, O. S., Womack, T. O., Flensburg, C., Keller, P., Paciorek, W., Sharff, A., Vonrhein, C., and Bricogne, G. (2012) Exploiting structure similarity in refinement: automated NCS and target-structure restraints in BUSTER. *Acta Crystallographica Section D: Biological Crystallography* **68**, 368-380
50. Datsenko, K. A., and Wanner, B. L. (2000) One-step inactivation of chromosomal genes in Escherichia coli K-12 using PCR products. *Proceedings of the National Academy of Sciences* **97**, 6640-6645
51. Baba, T., Ara, T., Hasegawa, M., Takai, Y., Okumura, Y., Baba, M., Datsenko, K. A., Tomita, M., Wanner, B. L., and Mori, H. (2006) Construction of Escherichia coli K-12 in-frame, single-gene knockout mutants: the Keio collection. *Molecular systems biology* **2**
52. Tu, Q., Yin, J., Fu, J., Herrmann, J., Li, Y., Yin, Y., Stewart, A. F., Müller, R., and Zhang, Y. (2016) Room temperature electrocompetent bacterial cells improve DNA transformation and recombineering efficiency. *Scientific reports* **6**, 24648

498 53. Doublet, B., Douard, G., Targant, H., Meunier, D., Madec, J.-Y., and Cloeckaert, A. (2008)
499 Antibiotic marker modifications of λ Red and FLP helper plasmids, pKD46 and pCP20, for
500 inactivation of chromosomal genes using PCR products in multidrug-resistant strains. *Journal*
501 *of microbiological methods* 75, 359-361

502

503

504 Figures

505

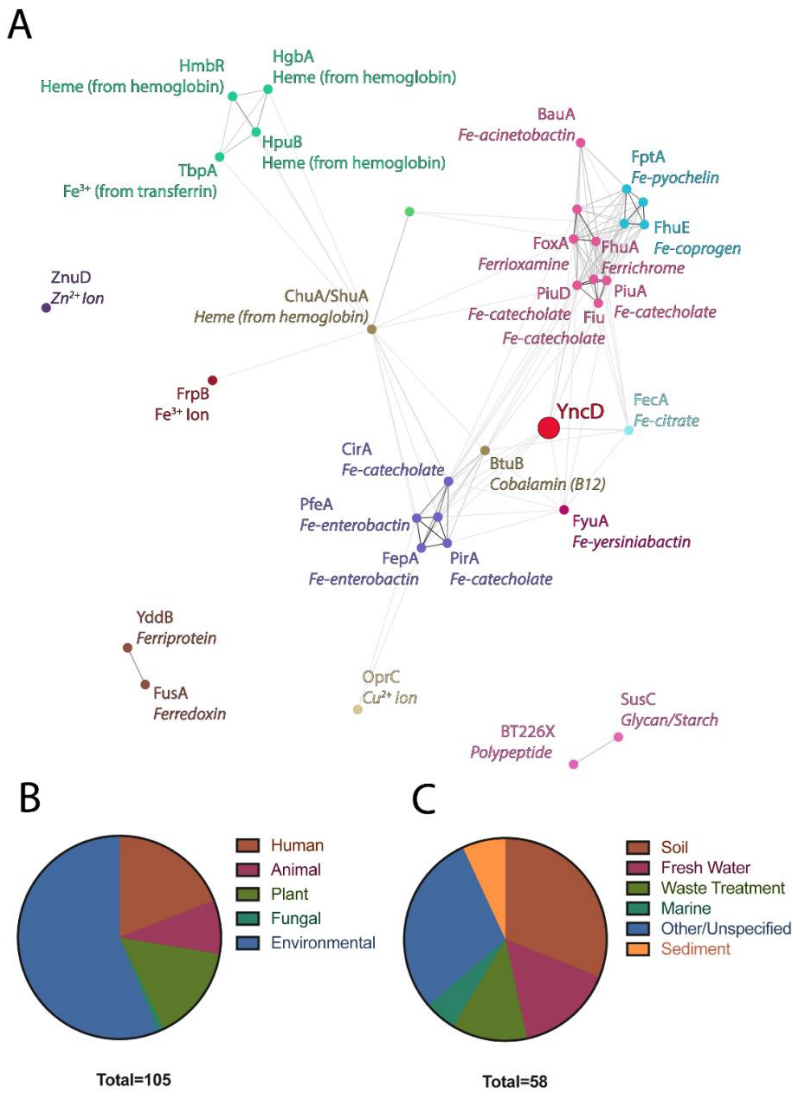

506

507

508

509 **Figure 1 The relationship between YncD and characterised TBDTs and the origin of bacteria**
510 **that possess YncD** (A) Sequence clustering analysis (E-value cutoff = 1×10^{-10}) of YncD with
511 TBDTs of known structure and/or function. Sequences are colored-coded according to the
512 sequence cluster to which they belong. The circle representing the sequence of YncD is
513 enlarged and colored red, showing that YncD does not cluster with other sequences. (B) The
514 environment or host of isolation of a subset of the YncD containing bacteria summarised in
515 Table S1. (C) The environment type of YncD containing bacterial isolates from environmental
516 sources.

517

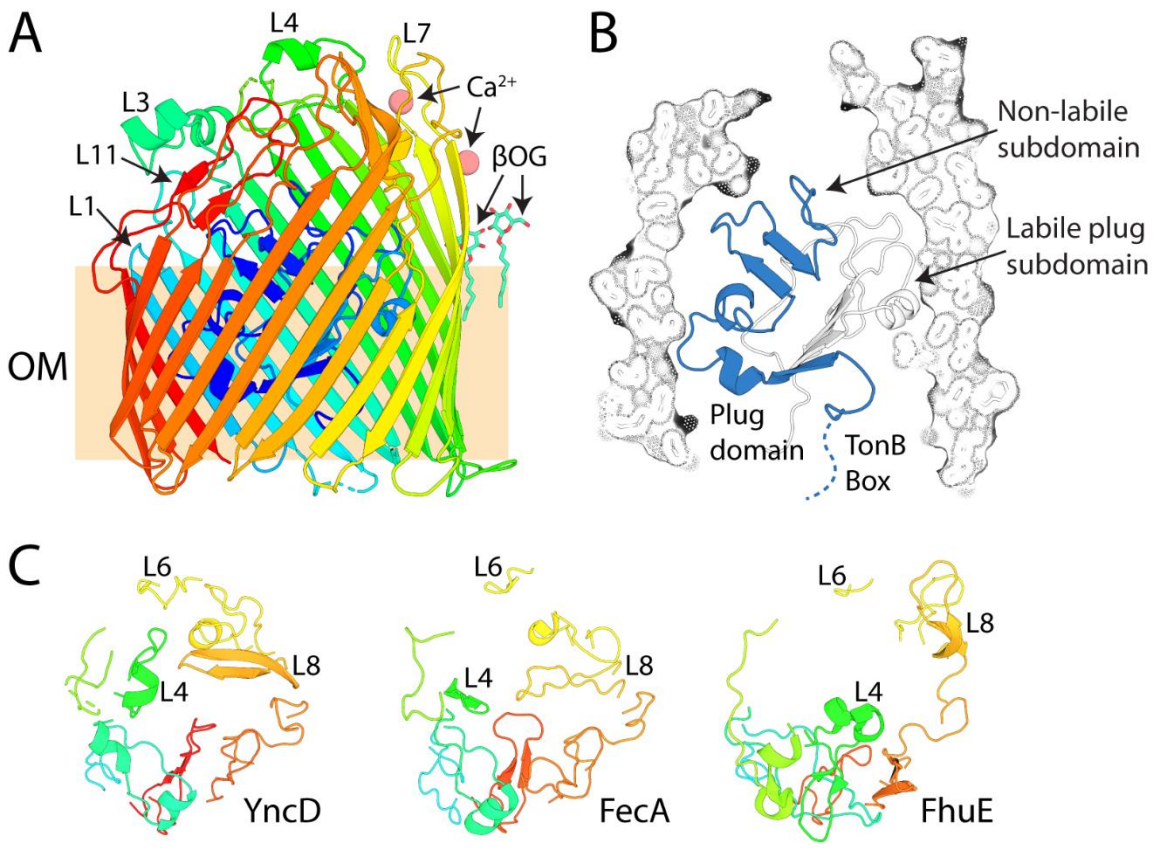

Figure 2 The crystal structure of YncD reveals structural homology to the distantly-related transporter FecA. (A) The crystal structure of YncD shown as a cartoon representation with rainbow coloring from the N-terminus (blue) to the C-terminus (red). Selected loops are labelled for reference i.e. L3 = Loop 3. The outer membrane-embedded region is boxed and with the label 'OM'. $Ca2^{+}$ ions and βOG detergent molecules co-crystallised with YncD are shown and sphere and stick representations respectively. (B) The crystal structure of YncD with the barrel domain shown as a cutaway surface and stick representation and the plug-domain shown as a cartoon representation. The labile section of the plug domain displaced by TonB is shown in blue, including the TonB box, which is disordered in the structure. (C) The extracellular loops of YncD, FecA (PDB ID = 1KMP) and FhuE (PDB ID = 6E4V) shown as a cartoon representation, with rainbow coloring as in panel A.

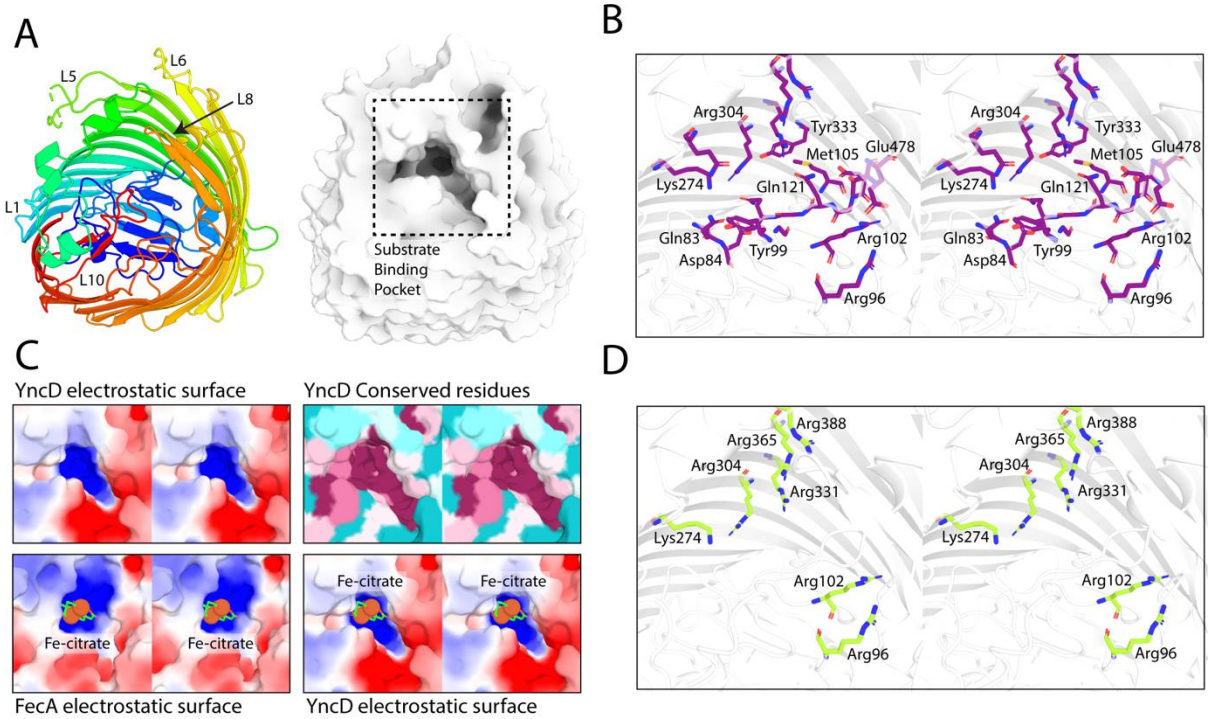

532

533

534 **Figure 3: YncD possesses a conserved positively charged substrate-binding pocket.** (A) A
535 cartoon representation of YncD colored as in Figure 1A (left) and a surface representation in
536 the same orientation showing the substrate-binding pocket (right). (B) A stereoview of the
537 amino acids in the YncD substrate-binding pocket which are conserved in YncD homologues
538 according to the program Consurf (33). The region shown corresponds to the boxed region in
539 panel A, YncD is shown as a cartoon representation and conserved residues are shown as
540 sticks. (C) A stereoview of the region of YncD from panel B shown as an electrostatic surface
541 (top left), as surface colored according to Consurf conservation scores: dark purple = highly
542 conserved, lighter purple = somewhat conserved, light blue = less conserved, dark blue =
543 poorly conserved (top right). An electron static surface of FecA in complex with Fe-citrate
544 shown as a stick and sphere representation (bottom left) and the position of Fe-citrate in the
545 YncD binding pocket when the FecA-Fe-citrate complex with superimposed with YncD
546 (bottom right). (D) A stereoview of positively charged conserved residues in the YncD
547 substrate-binding pocket.

548

549

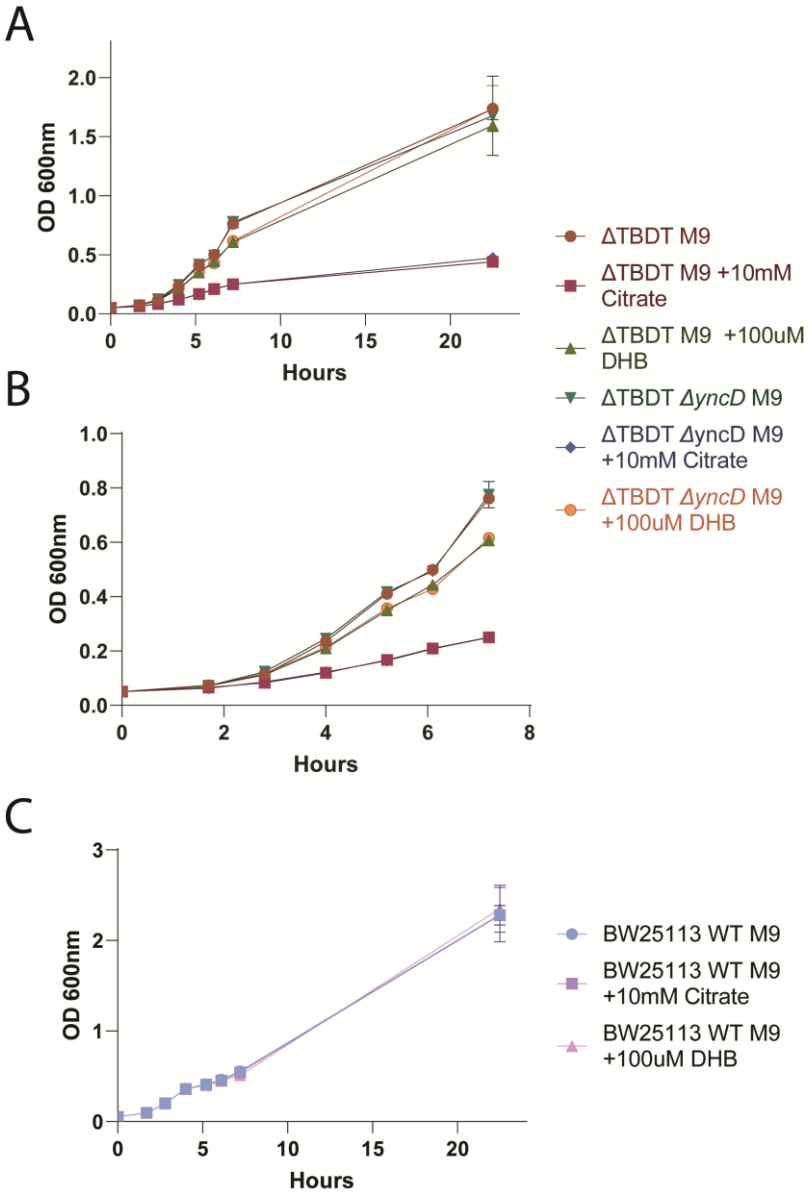

550

551 **Figure 4 YncD does not import ferric citrate or assist in iron acquisition under laboratory**
552 **conditions.** (A) A growth curve of E. *coli* ΔTBDT and E. *coli* ΔTBDT/*ΔyncD* grown in M9 minimal
553 media in the presence or absence of 10 mM citrate or 100 µM 2,3-dihydroxybenzoic acid. (B)
554 A zoomed view of the growth curve from panel A hours 1 to 7. (C) the growth of wildtype *E.*
555 *coli* BW25113 under the same conditions as the growth curve shown in panel A.

556

557 Table 1 YncD crystallography data collection and refinement statistics

	$K_2Pt(NO_2)_4$ Soak	Native
Data Collection[a]		
Space Group	*$P2_122_1$*	*$P2_122_1$*
Cell Dimensions		
a, b, c (Å)	90.61, 96.28, 127.39	87.85, 98.47, 124.70
α, β, γ (°)	90, 90, 90	90, 90, 90
Wavelength	0.9763	0.9763
Resolution (Å)	48.14-3.50 (3.83-3.50)	49.24-3.20 (3.42-3.20)
R_{merge}	38.6 (665.70)	28.1 (202.0)
R_{pim}	11.7 (201.2)	11.4 (79.7)
I/s(*I*)	7.6 (0.8)	7.9 (1.7)
CC(1/2)	0.999 (0.338)	0.998 (0.757)
Completeness (%)	99.8 (99.5)	100.0 (100.0)
Redundancy	22.1 (22.5)	13.2 (13.1)
No. unique reflections	14619 (3395)	18454 (3272)
Refinement statistics		
R_{work}/R_{free}		27.4/31.4
No. atoms		5127
Average B-factors		
Protein/Ligand		84.29, 77.10
R.m.s deviations		
Bond lengths (Å)		0.005
Bond angles (°)		0.735
Ramachandran Plot		
Favored/Allowed/Outliers (%)		94.1, 5.43, 0.47
PDB ID		6V81

[a] Values in parentheses are for the highest-resolution shell.

558